Giant enhanced four-wave mixing efficiency via two-photon resonance in asymmetric quantum wells

2015 Laser Phys. Lett. 12 095202

(http://iopscience.iop.org/1612-202X/12/9/095202)

IOP Publishing | Astro Ltd
Laser Physics Letters
Laser Phys. Lett. **12** (2015) 095202 (8pp)
doi:10.1088/1612-2011/12/9/095202

Giant enhanced four-wave mixing efficiency via two-photon resonance in asymmetric quantum wells

Shaopeng Liu[1], Wen-Xing Yang[1,2], Zhonghu Zhu[1] and Ray-Kuang Lee[2]

[1] Department of Physics, Southeast University, Nanjing 210096, People's Republic of China
[2] Institute of Photonics Technologies, National Tsing-Hua University, Hsinchu 300, Taiwan

E-mail: wenxingyang2@126.com

Received 17 July 2015
Accepted for publication 22 July 2015
Published 12 August 2015

Abstract

We propose an efficient four-wave mixing (FWM) scheme in asymmetric semiconductor quantum wells (SQWs) via two-photon resonance. By using the coupled Schrödinger–Maxwell formalism, we derive explicitly the corresponding analytical expressions of the inter-probe pulse and generated FWM field in the linear regime under the steady-state condition. With the aid of cross coupling between one ground state and two closely adjacent excited states, the efficiency of the generated FWM field is found to be significantly enhanced, up to 60%. More interestingly, a wide region of the maximum FWM efficiency is demonstrated as the ratio of transition dipole moments is within the values ranging from 1.1 to 1.3, which can be maintained for a certain propagation distance (i.e. 100 μm).

Keywords: four-wave mixing, semiconductor quantum wells, two-photon resonance

(Some figures may appear in colour only in the online journal)

1. Introduction

Over the past few decades, a great deal of nonlinear optical properties have been extensively investigated via the manipulation of quantum coherence and quantum interference. The motivation of such studies lies in the considerable potential applications, such as electromagnetically induced transparency (EIT) [1–5], lasing without population inversion [6, 7], enhanced nonlinearity [8–10] and Raman gain process [11, 12]. Associated with these nonlinear optical properties, a variety of interesting optical phenomena based on the quantum coherence and quantum interference effects have been demonstrated for optical solitons [13, 14], optical bistability (OB) and optical multistability (OM) [15], and the multi-wave mixing process [16–18]. In particular, numerous groups [19–25] have paid much attention to the multi-wave mixing process in EIT media, which have given rise to wide range of applications in diverse fields, including the high-efficiency generation of short-wave length coherent radiation, nonlinear spectroscopy with low-light intensity, quantum single-photon nonlinear optics and quantum information science [16–18, 26–35]. As an example, Deng *et al* [28] proposed a multi-wave mixing scheme by the ultraslow propagation of a pump field based on the dual EIT, and gained the enhanced conversion efficiency. Then, Wu and coworkers [27] analysed a four-wave mixing (FWM) scheme in a double-Λ system in the ultraslow propagation regime and the maximum FWM efficiency was greater than 25%. More recently, Sun *et al* [25] suggested and achieved a highly efficient FWM scheme in an asymmetric double quantum well structure with resonant tunneling. However, the low conversion efficiency for multi-wave mixing has so far been restricted to its applications.

On the other hand, the semiconductor quantum wells (SQWs) appear to be a good candidate for providing large electric dipole moments based on intersubband transitions (ISBTs), due to the small effective electron mass, high nonlinear optical coefficient, and great flexibility in device design by choosing the materials and structure dimensions. Specifically, the SQW system has the more accessible cross coupling between optical transitions, which arises from two transitions between one ground state and two closely spaced

excited states coupling by a continuous-wave (cw) control field. This cross coupling can modify the linear and nonlinear optical responses of another probe pulsing transition and trigger a strong coherence between the two closely spaced excited states. To the best of our knowledge, although the cross coupling has been applied to investigating slow dark optical solitons [36], a significant gain [37] and enhanced Kerr nonlinearities [38]; the enhanced multi-wave mixing scheme in asymmetric quantum wells by cross coupling between optical transitions has been unexplored.

In this paper, we propose and analyse a highly efficient FWM scheme in a five-subband SQW configuration. By solving the coupled Schrödinger–Maxwell equations, we obtain the corresponding explicit analytical expressions for the probe pulse, the generated FWM pulse field, the phase shifts and absorption coefficients, as well as the conversion efficiency of the FWM. Differently to the previous scheme, we implement a two-photon resonance scheme to induce FWM processes driven by one weak probe pulse interacting with two cw pump fields. Owing to the existence of cross coupling between optical transitions, a novel wave-mixing channel may be opened and the maximum FWM conversion efficiency can be dramatically enhanced, up to 60%. Last but not least, a wide region of the maximum FWM efficiency is demonstrated as the ratio of transition dipole moments is within the values ranging from 1.1 to 1.3, which can be maintained for a certain propagation distance (i.e. 100 μm).

2. The theoretical model and basic equations

The SQW structure with the relevant band energy levels and wave functions, which is associated with intersubband transitions(ISBTs), is shown in figure 1. The material of the SQW structure can be demonstrated as follows. The left shallow well and right deep well consist of an $Al_{0.04}Ga_{0.96}As$ layer with a thickness of 11.0 nm and a 9.5 nm GaAs layer, which are separated by a 3.8 nm $Al_{0.4}Ga_{0.6}As$ potential barrier. Both the left side of shallow well and the right side of deep well are $Al_{0.4}Ga_{0.6}As$ potential barriers. The eigenenergies of the five conduction subbands can be obtained by solving the effective mass Schrödinger equations. Thus, the energies of the two ground subbands $|1\rangle$ and $|2\rangle$ are obtained as $E_1 = 34.5$ meV and $E_2 = 62.3$ meV, respectively. Two closely spaced delocalised subbands $|3\rangle$ and $|4\rangle$ with the eigenenergies $E_3 = 135.5$ meV and $E_4 = 141.5$ meV are separated by the splitting 2Δ (see figure 1(b)), which lies in between the two ground subbands and the subband $|5\rangle$. The energy of second excited subband $|5\rangle$ is 296.3 meV in the right deep well. As shown in figure 1(a), the dashed lines represent the relevant energy levels while the solid curves show the corresponding wave functions for the five subbands. The SQW system is driven by a weak probe pulse (central frequency ω_p and wave vector k_p) via the excited subbands $|3\rangle$ and $|4\rangle$, while $|3\rangle$ and $|4\rangle$ are coupled with the subbands $|2\rangle$ and $|5\rangle$ by two continuous-wave (cw) control fields (central frequencies ω_{c1}, ω_{c2} and wave vectors k_{c1}, k_{c2}), then generates a FWM pulse field (central frequency ω_m and wave vector k_m). The process based on IBTS contains the transitions $|1\rangle \leftrightarrow |3\rangle, |1\rangle \leftrightarrow |4\rangle, |2\rangle \leftrightarrow |3\rangle, |2\rangle \leftrightarrow |4\rangle, |2\rangle \leftrightarrow |5\rangle$ and $|5\rangle \leftrightarrow |1\rangle$. In the present analysis, we use the following conditions: (1) to reduce the electron–electron effects, the quantum well structure is designed with a low electron sheet density, so that it is reasonable to neglect the electron–electron interactions; (2) all the subbands have the same effective mass.

In the interaction picture, with the rotating-wave approximation and the electric-dipole approximation, the interaction Hamiltonian of the system under study can be written as ($\hbar = 1$):

$$\begin{aligned} H_{\rm int}^I/\hbar = {} & (\Delta_p - \Delta_{c1})|2\rangle\langle 2| + (\Delta_p - \Delta)|3\rangle\langle 3| \\ & + (\Delta_p + \Delta)|4\rangle\langle 4| + (\Delta_{c2} + \Delta_p - \Delta_{c1})|5\rangle\langle 5| \\ & - (g\Omega_p e^{ik_p\cdot r}|3\rangle\langle 1| + \Omega_p e^{ik_p\cdot r}|4\rangle\langle 1| + f\Omega_{c1}e^{ik_{c1}\cdot r}|3\rangle\langle 2| + \text{h.c.}) \\ & - (\Omega_{c1}e^{ik_{c1}\cdot r}|4\rangle\langle 2| + \Omega_{c2}e^{ik_{c2}\cdot r}|5\rangle\langle 2| + \Omega_m e^{ik_m\cdot r}|5\rangle\langle 1| + \text{h.c.}), \end{aligned} \tag{1}$$

where $\Delta_p = \left(\frac{E_3+E_4}{2} - E_1\right) - \omega_p$, $\Delta_{c1} = \left(\frac{E_3+E_4}{2} - E_2\right) - \omega_{c1}$ and $\Delta_{c2} = E_5 - E_2 - \omega_{c2}$ denote the corresponding field detunings, while $2\Delta = E_4 - E_3$ represents the energy splitting between the subbands $|3\rangle$ and $|4\rangle$, in which $\omega_i (i = p, c1, c2, m)$ are the optical frequencies of the relevant optical fields and $k_j (j = p, c1, c2, m)$ are the wave vectors of the probe pulse, two continuous wave laser fields and the generated FWM field. $\Omega_n (n = p, c1, c2, m)$ are one-half Rabi frequencies for the relevant laser-driven intersubband transitions, i.e. $\Omega_p = \mu_{41}E_p/2\hbar$, $\Omega_{c1} = \mu_{42}E_{c1}/2\hbar$, $\Omega_{c2} = \mu_{52}E_{c2}/2\hbar$ and $\Omega_m = \mu_{51}E_m/2\hbar$, while $g = \mu_{31}/\mu_{41}$ and $f = \mu_{32}/\mu_{42}$ represent the ratios of the transition dipole moments between the relevant subbands, where $\mu_{ij} (i, j = 1 - 5; i \neq j)$ denote the dipole moments for the transition between subbands $|i\rangle \leftrightarrow |j\rangle$ and $E_{p,\,c1,\,c2,\,m}$ are the slowly varying electric field amplitudes of the corresponding fields.

We assume that the wave function of the system is $|\Psi\rangle = A_1|1\rangle + A_2 e^{i(k_p - k_{c1})\cdot r}|2\rangle + A_3 e^{ik_p\cdot r}|3\rangle + A_4 e^{ik_p\cdot r}|4\rangle + A_5 e^{i(k_p - k_{c1} + k_{c2})\cdot r}|5\rangle$, where $A_j (j = 1 - 5)$ means the time-dependent probability amplitudes of the particle in the corresponding subbands. By substituting $|\Psi\rangle$ into the Schrödinger equation $i\partial\Psi/\partial t = H_{\rm int}^I\Psi$, the equations of motion for the probability amplitude can be written as

$$i\frac{\partial A_1}{\partial t} = -g\Omega_p^* A_3 - \Omega_p^* A_4 - \Omega_m^* A_5 e^{i\delta k\cdot r}, \tag{2}$$

$$i\frac{\partial A_2}{\partial t} = d_2 A_2 - f\Omega_{c1}^* A_3 - \Omega_{c1}^* A_4 - \Omega_{c2}^* A_5, \tag{3}$$

$$i\frac{\partial A_3}{\partial t} = d_3 A_3 - g\Omega_p A_1 - f\Omega_{c1} A_2, \tag{4}$$

$$i\frac{\partial A_4}{\partial t} = d_4 A_4 - \Omega_p A_1 - \Omega_{c1} A_2, \tag{5}$$

$$i\frac{\partial A_5}{\partial t} = d_5 A_5 - \Omega_{c2} A_2 - \Omega_m e^{-i\delta k\cdot r} A_1, \tag{6}$$

here we have introduced the new definitions $d_2 = (\Delta_p - \Delta_{c1}) - i\gamma_2, d_3 = (\Delta_p - \Delta) - i\gamma_3, d_4 = (\Delta_p + \Delta) - i\gamma_4,$

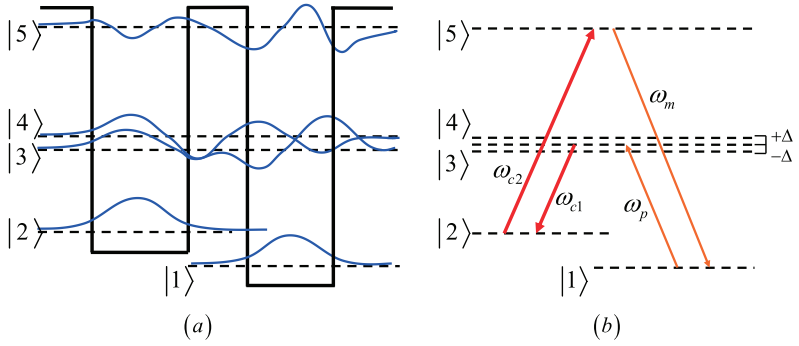

Figure 1. (a) Schematic band diagram of the asymmetric semiconductor quantum wells with a deep well and a shallow well, which mix to create five subbands $|j\rangle$ ($j = 1$–5). The related energy levels and the corresponding wave functions are illustrated by the dashed and solid lines, respectively. (b) Schematic of the relevant energy levels with a five-subband $|j\rangle$ configuration. Accurately, the ground state $|1\rangle$ is driven by a weak probe pulse (frequency ω_p and Rabi frequency $2\Omega_p$) via excited subbands $|3\rangle$ and $|4\rangle$, while the $|3\rangle$ and $|4\rangle$ are coupled with the subbands $|2\rangle$ and $|5\rangle$ by two continuous-wave (cw) control fields (frequencies ω_{c1}, ω_{c2} and Rabi frequencies $2\Omega_{c1}$, $2\Omega_{c2}$).

$d_5 = (\Delta_{c2} + \Delta_p - \Delta_{c1}) - i\gamma_5$. The $\delta k = k_p - k_{c1} + k_{c2} - k_m$ denotes the phase mismatching factor. The decay rates can be phenomenologically included in the above equations. In SQW, the total decay rates γ_i of subband $|i\rangle$ comprise the population decay rates γ_{il} and the pure dipole dephasing rates γ_{id}, i.e. $\gamma_i(i = 1 - 5) = \gamma_{il} + \gamma_{id}$, where the population decay rates γ_{il} are primarily due to the longitudinal optical photon emission events at low temperature and the pure dipole dephasing rates γ_{id} are assumed to be a combination of quasi-elastic interface roughness scattering or acoustic photon scattering. Moreover, the dipole transition rate from subband $|2\rangle$ to $|1\rangle$ is very small because of the high inter-well barrier, i.e. $\gamma_2 = \gamma_{2d}$.

In order to predict correctly the propagation of the input probe pulse and the generated FWM field, the probability amplitudes of the above equations (2)–(6) must be simultaneously solved with Maxwells equation in a self-consistent manner. Under the slowly varying amplitude approximation, the input probe and the generated FWM field propagating along the direction of z (i.e. $\delta k \cdot r = \delta k \cdot z$) evolve according to

$$\frac{\partial \Omega_p}{\partial z} + \frac{1}{c}\frac{\partial \Omega_p}{\partial t} = i\kappa_p(gA_3 + A_4)A_1^*, \tag{7}$$

$$\frac{\partial \Omega_m}{\partial z} + \frac{1}{c}\frac{\partial \Omega_m}{\partial t} = i\kappa_m A_5 A_1^*. \tag{8}$$

For the sake of simplicity, we assume phase mismatching factor $\delta k = 0$. The parameters $\kappa_p = 2\pi N\omega_p |\mu_{31}|^2/\hbar c$ and $\kappa_m = 2\pi N\omega_m |\mu_{51}|^2/\hbar c$ are the propagation constants with the electron concentration N. The standard method of the weak nonlinear theory can be usefully applied to solve the nonlinear equations, that is, we assume the Rabi frequency Ω_p of the input probe pulse is comparatively very weak ($|\Omega_p| \ll |\Omega_{c1,c2}|$) so that almost all the electrons will remain in subband $|1\rangle$ i.e. $A_1 \simeq 1$. Simultaneously, we preform the Fourier transformations for equations (2)–(8),

$$A_j(t) = \frac{1}{\sqrt{2\pi}}\int_{\infty}^{\infty} a_j(\omega)e^{-i\omega t}d\omega, j = 2, 3, 4, 5, \tag{9}$$

$$\Omega_{p,m}(t) = \frac{1}{\sqrt{2\pi}}\int_{\infty}^{\infty} \Lambda_{p,m}(\omega)e^{-i\omega t}d\omega, \tag{10}$$

with ω being the Fourier transform variable, we have

$$(\omega - d_2)a_2 + f\Omega_{c1}^* a_3 + \Omega_{c1}^* a_4 + \Omega_{c2}^* a_5 = 0, \tag{11}$$

$$(\omega - d_3)a_3 + f\Omega_{c1}a_2 = -g\Lambda_p, \tag{12}$$

$$(\omega - d_4)a_4 + \Omega_{c1}a_2 = -\Lambda_p, \tag{13}$$

$$(\omega - d_5)a_5 + \Omega_{c2}a_2 = -\Lambda_m, \tag{14}$$

$$\frac{\partial \Lambda_p}{\partial z} - i\frac{\omega}{c}\Lambda_p = i\kappa_p(ga_3 + a_4)a_1^*, \tag{15}$$

$$\frac{\partial \Lambda_m}{\partial z} - i\frac{\omega}{c}\Lambda_m = i\kappa_m a_5 a_1^*, \tag{16}$$

where a_{2-5} and Λ_p and Λ_m are the Fourier transforms of A_{2-5}, Ω_P and Ω_m, respectively. The solutions of the equations (11)–(14) are noted

$$ga_3 + a_4 = \frac{D_{P1}(\omega)}{D(\omega)}\Lambda_p + \frac{D_{m1}(\omega)}{D(\omega)}\Lambda_m, \tag{17}$$

$$a_5 = \frac{D_{p2}(\omega)}{D(\omega)}\Lambda_p + \frac{D_{m2}(\omega)}{D(\omega)}\Lambda_m, \tag{18}$$

here we have introduced the definitions $D_{p1}(\omega)$, $D_{m1}(\omega)$, $D_{p2}(\omega)$, $D_{m2}(\omega)$ and $D(\omega)$, which can be expressed as $D_{p1}(\omega) = [(\omega - d_3) + g^2(\omega - d_4)][(\omega - d_2)(\omega - d_5) - \Omega_{c2}^2] - \Omega_{c1}^2(\omega - d_5)(f - g)^2$, $D_{m1}(\omega) = (\omega - d_3)\Omega_{c1}\Omega_{c2}^* + gf\Omega_{c1}\Omega_{c2}^*(\omega - d_4)$, $D_{p2}(\omega) = (\omega - d_3)\Omega_{c1}^*\Omega_{c2} + gf\Omega_{c1}^*\Omega_{c2}(\omega - d_4)$, $D_{m2}(\omega) = (\omega - d_2)(\omega - d_3)(\omega - d_4) - \Omega_{c1}^2(\omega - d_3) + (\omega - d_4)f^2\Omega_{c1}^2$ and $D(\omega) = (\omega - d_3)(\omega - d_4)\Omega_{c2}^2 + (\omega - d_3)(\omega - d_5)\Omega_{c1}^2 + f^2(\omega - d_4)(\omega - d_5)\Omega_{c1}^2 - (\omega - d_2)(\omega - d_3)(\omega - d_4)(\omega - d_5)$. Making the initial condition of the probe pulse and generated FWM field, i.e. $\Lambda_p(0,\omega)$ and $\Lambda_m(0,\omega) = 0$ and applying the equations (15) and (16) and equations (17) and (18), we obtain the solutions as follows

$$\Lambda_p(z, \omega) = \Lambda_p(0, \omega)(U_+(\omega)e^{izK_+(\omega)} - U_-(\omega)e^{izK_-(\omega)}), \tag{19}$$

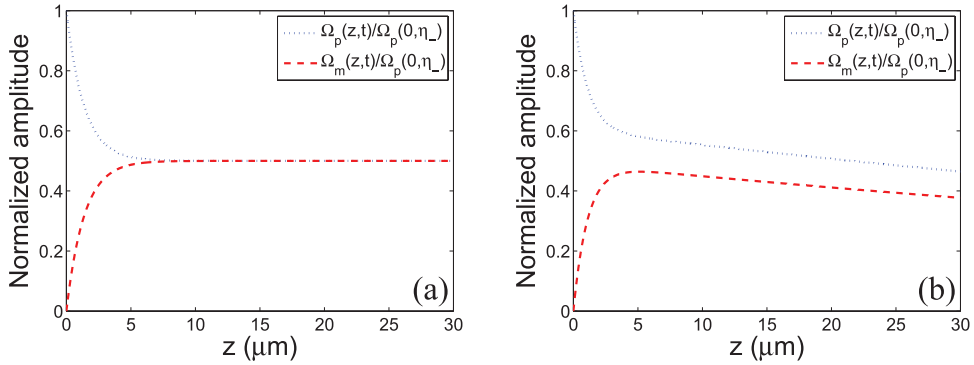

Figure 2. The amplitudes of the probe pulse and the generated FWM field versus the depth z of penetration in the SQW system with the different ratio values of transition dipole moments: (a) $g = 1.2$, (b) $g = 1.6$. The other parameter values are $\gamma_2 = 2\times10^{-5}$ meV, $\gamma_3 = \gamma_4 = 9$ meV, $\gamma_5 = 4$ meV, $\Delta = 3.5$ meV, $\Delta_p = \Delta_{c1} = \Delta_{c2} = 0$, $\kappa_p = \kappa_p = 3\,\mu\mathrm{m}^{-1}$ meV and $|\Omega_{c1}| = |\Omega_{c2}| = 20$ meV.

$$\Lambda_m(z,\omega) = \Lambda_p(0,\omega)S(\omega)(\mathrm{e}^{\mathrm{i}zK_+(\omega)} - \mathrm{e}^{\mathrm{i}zK_-(\omega)}), \tag{20}$$

where

$$K_\pm(\omega) = \frac{\omega}{c} + \frac{D_{m2}(\omega)\kappa_m + D_{p1}(\omega)\kappa_p \mp \sqrt{G(\omega)}}{2D(\omega)} = K_\pm(0) + K_\pm^{(1)}(\omega) + o(\omega^2),$$

$$U_\pm(\omega) = \frac{D_{P1}(\omega)\kappa_p - D_{m2}(\omega)\kappa_m \pm \sqrt{G(\omega)}}{2\sqrt{G(\omega)}} = U_\pm(0) + o(\omega),$$

$$S(\omega) = \frac{\kappa_m D_{p2}(\omega)}{\sqrt{G(\omega)}} = S(0) + o(\omega),$$

with $G(\omega) = (D_{m2}(\omega)\kappa_m - D_{p1}(\omega)\kappa_p)^2 + 4D_{m1}(\omega)D_{p2}(\omega)\kappa_m\kappa_p$. $\Lambda_{p,m}(0,\omega)$ are the initial conditions for the probe pulse and the generated FWM field at the entrance of the SQW structures $z = 0$. Equations (19) and (20) demonstrate clearly that there exist two modes ($K_\pm$ modes) described by the linearised dispersion relations $K = K_+(\omega)$ and $K = K_-(\omega)$, respectively. In the following, we focus on the adiabatic regime, where the expressions of the probe pulse and the generated FWM field are expanded into a rapid conversion power series around the centre frequencies $\omega_{p,s}$ (i.e. $\omega = 0$). In order to analyse the expressions of the probe pulse and the generated FWM field, the approximation is applied by neglecting the high order terms, i.e. $O(\omega^2)$ in $K_\pm(\omega)$ and $O(\omega)$ in $S(\omega)$, respectively. Generally, $\mathrm{Re}[K_\pm(0)]$ represent the phase shifts per unit length, and $\mathrm{Im}[K_\pm(0)]$ are the absorption coefficients. The group velocities $V_{g\pm}$ of the two modes are determined by $V_{g\pm} = 1/\mathrm{Re}[K_\pm^{(1)}]$. Subsequently, we applied an inverse Fourier transform to $\Lambda_{p,m}$

$$\Omega_{p,m}(z,t) = \frac{1}{\sqrt{2\pi}}\int_{-\infty}^{\infty}\exp(-\mathrm{i}\omega t)\Lambda_{p,m}(z,\omega)\,\mathrm{d}\omega.$$

We can achieve the linearised results of the probe pulse and the generated FWM field

$$\Omega_p(z,\omega) = \Omega_p(0,\eta_+)U_+(0)\mathrm{e}^{\mathrm{i}zK_+(0)} - \Omega_p(0,\eta_-)U_-(0)\mathrm{e}^{\mathrm{i}zK_-(0)}, \tag{21}$$

$$\Omega_m(z,\omega) = S(0)(\Omega_p(0,\eta_+)\mathrm{e}^{\mathrm{i}zK_+(0)} - \Omega_p(0,\eta_-)\mathrm{e}^{\mathrm{i}zK_-(0)}), \tag{22}$$

where $\eta_\pm = t - z/V_{g\pm}$. $\Omega_p(t) \equiv \Omega_p(z=0,t)$ is the initial probe pulse at $z = 0$. The above two equations (21) and (22) are the accurate expressions that govern the propagation dynamics of the probe pulse and the generated FWM field in the present SQW system. In such a feasible case, the enhancement of the FWM signal can be achieved by properly adjusting the system parameters via cross coupling between optical transitions.

3. The numerical results and discussions

In the case of high-quality SQW, for temperatures up to 10 K [39], the electric density keeps below $10^{24}\mathrm{m}^{-3}$. The typical decay parameters are chosen as $\gamma_2 = 2\times10^{-5}$ meV, $\gamma_{3l} = \gamma_{4l} = 7.8$ meV, $\gamma_{5l} = 3$ meV, $\gamma_{3d} = \gamma_{4d} = 1.2$ meV and $\gamma_{5d} = 1$ meV, as a result, we can obtain $\gamma_3 = \gamma_4 = 9$ meV and $\gamma_5 = 4$ meV. In addition, we choose $\Delta_p = \Delta_{c1} = \Delta_{c2} = 0$ and $\kappa_p = \kappa_m = 3\ \mu\mathrm{m}^{-1}$ meV. Here, the two-photon resonance occurs in the intersubband transition $|1\rangle \leftrightarrow |2\rangle$ (i.e. $\Delta_p + \Delta_{c1} = 0$). Within these parameter regimes, we plot the amplitudes of the probe pulse and the generated FWM field versus the depth z of penetration in the SQW system with the different ratio values of the transition dipole moments in figure 2. For the one case where the ratio value of the transition dipole moments $g = 1.2$ in figure 2(a), it can be seen that the amplitude of the probe pulse decreases monotonically with the increase in the propagation distance z, while the generated FWM field increases monotonically. When the propagation distance z continues to extend, the amplitudes of the generated FWM fields reach the saturation value and are independent of the propagation z. These results can be explained by the behaviour of the multiphoton quantum destructive interference between the two different excitation channels: coupling excitation pathways $|1\rangle \to |3\rangle$, $|1\rangle \to |4\rangle$ and feedback excitation pathways $|1\rangle \to |3\rangle$, $|1\rangle \to |4\rangle$ mediated by $|5\rangle$ [35]. Physically, when the amplitude of the generated FWM field reaches a saturation value whereby the generated FWM field is sufficiently intense, an efficient feedback excitation pathway to the subband $|5\rangle$ becomes important, which is π out of phase with respect to the coupling excitation pathway. Then

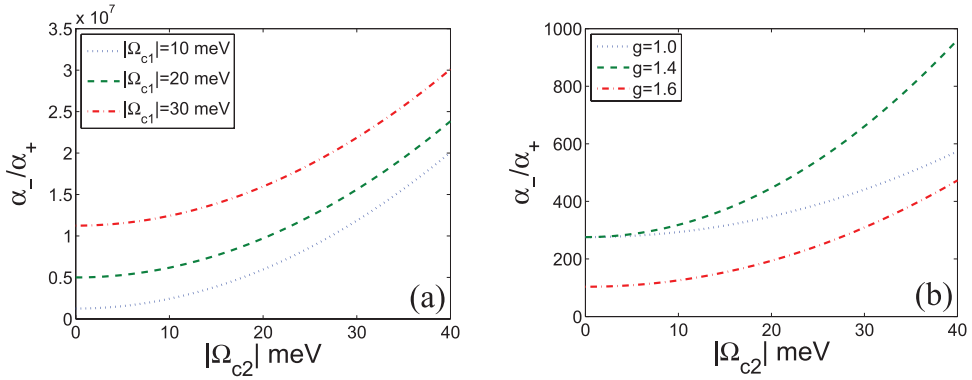

Figure 3. (a) The ratio of the absorption coefficients α_-/α_+ versus the amplitude $|\Omega_{c2}|$ of the cw control field for the ratio of the transition dipole moments $g = 1.2$ as fixed and the other amplitude $|\Omega_{c1}| = 10$ meV, 20 meV and 30 meV. (b) The ratio of the absorption coefficients α_-/α_+ versus the amplitude $|\Omega_{c2}|$ for the other amplitude $|\Omega_{c1}| = 20$ meV as fixed and the ratio of transition dipole moments $g = 1.0$, 1.4, 1.6. The other parameter values are $f = 1.2$, $\gamma_2 = 2\times10^{-5}$ meV, $\gamma_3 = \gamma_4 = 9$ meV, $\gamma_5 = 4$ meV, $\Delta = 3.5$ meV, $\Delta_p = \Delta_{c1} = \Delta_{c2} = 0$ and $\kappa_p = \kappa_p = 3$ μm^{-1} meV.

the amplitude of the generated FWM field was suppressed due to the feedback excitation pathway leading to multi-photon destructive interference. For the other case where the ratio value of the transition dipole moments $g = 1.6$ in figure 2(b), the two amplitudes of the probe pulse and the generated FWM field show an obvious gap and attenuation after a certain propagation distance. As a matter of fact, the linear absorption–dispersion properties of the SQW medium play an important role in the above phenomenon. When the ratio value of the transition dipole moment g is far from f, the according absorption increases rapidly, so that the amplitudes of the probe pulse and generated FWM field decay rapidly.

Both equations (21) and (22) can demonstrate that the two modes (i.e. $K_\pm$ modes) exist in the SQW system, which are contained in the probe pulse and FWM field. By comparing the two absorption coefficients $\alpha_\pm = \mathrm{Im}[K_\pm(0)]$, the key consequence is that one of the modes always decays much faster than the other, resulting in the neglect of the fast decaying mode after a short propagation distance. To give a clear illustration, figure 3(a) plots the absorption coefficient ratio α_-/α_+ versus the amplitude $|\Omega_{c2}|$ of the cw control field, while we show the absorption coefficient ratio α_-/α_+ versus the amplitude $|\Omega_{c2}|$ for several different ratios g of the transition dipole moments in figure 3(b). When the two ratios of the transition dipole moments are within appropriate parameter ranges, figures 3(a) and (b) show directly that the ratio of the absorption coefficients increases monotonously with the increase in the amplitudes of the two cw pump fields. The absorption coefficients satisfy $\alpha_+ \ll \alpha_-$, which can be also obtained in figure 3. That is to say, the K_- mode decays more quickly than the K_+ mode, thus the faster variable K_- can be neglected safely after a short characteristic propagation distance. In a word, the above approximation method can be implemented, as long as the ratio g of the transition dipole moments is confined from 1.0 to 1.6. In the following discussion, we present all of the results under the condition of approximation. This is indeed the case for the situations considered here. Specifically, under this approximation of neglecting the K_- mode, the probe pulse and generated FWM field $\Omega_{p,m}$ can be rewritten as

$$\Omega_p(z,t) = \Omega_p(0, t - z/V_g)U_+(0)\mathrm{e}^{\mathrm{i}z\beta - z\alpha}, \tag{23}$$

$$\Omega_m(z,t) = \Omega_p(0, t - z/V_g)S(0)\mathrm{e}^{\mathrm{i}z\beta - z\alpha}, \tag{24}$$

where $V_g = 1/\mathrm{Re}[K_+^{(1)}]$ is the group velocity, $\alpha = \mathrm{Im}[K_+(0)]$ denotes the absorption coefficient, and $\beta = \mathrm{Re}[K_+(0)]$ represents the phase shift per unit length. On applying the definition of [27], the efficiency of the generated FWM field can be derived, i.e. $\rho = \left|E_m^{(\mathrm{out})}/E_p^{(\mathrm{in})}\right|$, where $E_m^{(\mathrm{out})}$ is the electric field $E_m(|E_m|^2 = 4\hbar^2\,|\Omega_m|^2/|\mu_{51}|^2)$ of the FWM-generated field at the exit $z = L$ and $E_p^{(in)}(\left|E_p\right|^2 = 4\hbar^2\,\left|\Omega_p\right|^2/|\mu_{41}|^2)$ is the electric field of the probe pulse at the entrance $z = 0$. According to equations (23) and (24), the efficiency has the form,

$$\rho = \left(\frac{E_m^{(\mathrm{out})}}{E_p^{(\mathrm{in})}}\right)^2 = \frac{\mu_{41}^2}{\mu_{51}^2}\frac{(\kappa_m^2\Omega_{c1}^2\Omega_{c2}^2A^2)}{4\kappa_p\kappa_m\Omega_{c1}^2\Omega_{c2}^2A^2 + B^2}\mathrm{e}^{-2\alpha L}, \tag{25}$$

with $A = (gf\Delta - \Delta - \mathrm{i}\gamma_3 - \mathrm{i}gf\gamma_4)$ and $B = \kappa_m{\Omega_{c1}}^2(\Delta - f^2\Delta + \mathrm{i}\gamma_3 + \mathrm{i}f^2\gamma_4) - \kappa_p{\Omega_{c2}}^2(\Delta - g^2\Delta + \mathrm{i}\gamma_3 + \mathrm{i}g^2\gamma_4) - \mathrm{i}\kappa_p(f-g)^2{\Omega_{c1}}^2\gamma_5$ By means of the relation $\mu_{41}^2/\mu_{51}^2 = \kappa_p\omega_m/\kappa_m\omega_p$, it is found that the expression of the efficiency ρ can be simplified as $\rho = (\omega_m\mathrm{e}^{-2\alpha L})/4\omega_p$. In the following, we present a few numerical results for the dependence of the generated FWM efficiency on different parameters of the system, as illustrated in figures 4–7.

First of all, we will analyse how the amplitudes of the cw pump fields modify the efficiency of the generated FWM field. In order to demonstrate this explicitly, in figure 4 we plot the FWM efficiency ρ as a function of the amplitude $|\Omega_{c2}|$ of the cw pump field for the different cw pump field $|\Omega_{c1}|$ by adjusting the ratio value g of the transition dipole moments, while keeping all the other parameters fixed. It can be seen that the maximum efficiency is achieved under the condition $|\Omega_{c1}| = |\Omega_{c2}|$ and the maximum efficiencies have exceed 50% both figures 4(a) and (b). If our SQW system does not contain the subband $|4\rangle$, the scheme is simplified, as in the scheme of Wu [27], in which the maximum efficiency of the FWM field has just half of our scheme. In other words, the giant

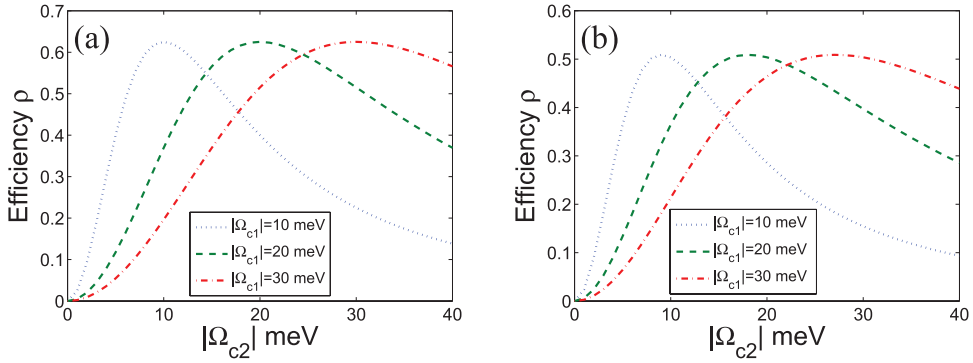

Figure 4. The generated FWM efficiency ρ versus the amplitude $|\Omega_{c2}|$ for $|\Omega_{c1}|$= 10 meV, 20 meV and 30 meV: (a) $g = 1.2$, (b) $g = 1.6$. The other parameter values are $f = 1.2$, $L = 10\ \mu$m, $\gamma_2 = 2 \times 10^{-5}$ meV, $\gamma_3 = \gamma_4 = 9$ meV, $\gamma_5 = 4$ meV, $\Delta = 3.5$ meV, $\Delta_p = \Delta_{c1} = \Delta_{c2} = 0$ and $\kappa_p = \kappa_p = 3\ \mu\text{m}^{-1}$ meV.

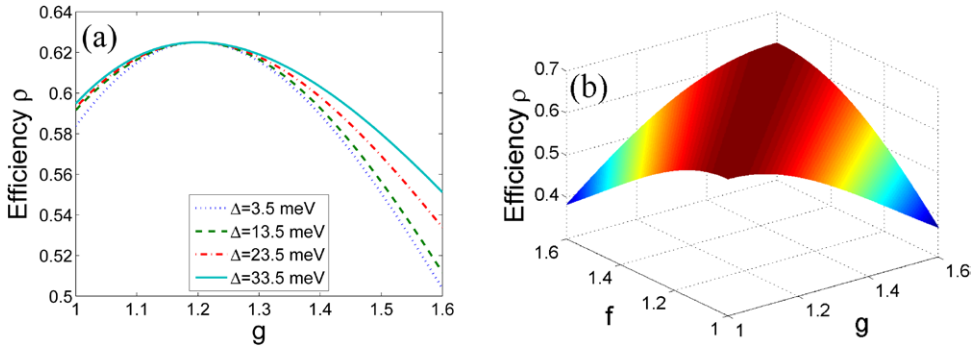

Figure 5. (a) The conversion efficiency ρ of the generated FWM field versus the ratio g of the transition dipole moments for different energy splitting $\Delta = 3.5$ meV, $\Delta = 13.5$ meV, $\Delta = 23.5$ meV, $\Delta = 33.5$ meV. (b) The conversion efficiency ρ of the generated FWM field as a function of the two ratios of transition dipole moments (i.e g and f) with $\Delta = 3.5$ meV. The other parameter values are $f = 1.2$, $L = 10\ \mu$m, $\gamma_2 = 2 \times 10^{-5}$ meV, $\gamma_3 = \gamma_4 = 9$ meV, $\gamma_5 = 4$ meV, $\Delta_p = \Delta_{c1} = \Delta_{c2} = 0$, $\kappa_p = \kappa_p = 3\ \mu\text{m}^{-1}$ meV and $|\Omega_{c1}| = |\Omega_{c2}| = 20$ meV.

enhanced FWM efficiency can be observed when the cross coupling between optical transitions are included in the asymmetric quantum wells. This cross coupling driven by two transitions between one ground and two closely separated excited states can induce the two generated FWM processes (i.e. $|1\rangle \rightarrow |3\rangle \rightarrow |2\rangle \rightarrow |5\rangle \rightarrow |1\rangle$ and $|1\rangle \rightarrow |4\rangle \rightarrow |2\rangle \rightarrow |5\rangle \rightarrow |1\rangle$). Simultaneously, the new channel is opened to modify the linear absorption of the SQW medium, which leads to the giant enhancement of the FWM efficiency. More interestingly, a direct comparison of the results in figures 4(a) and (b) implies that the conversion efficiency can be obviously enhanced when we go from $g = 1.6$ (see figure 4(b)) to $g = 1.2$ (see figure 4(a)). The reason is that, with the decrease in the ratio g of the transition dipole moments, the absorption for the FWM-generated field on the intersubband transition $|1\rangle \leftrightarrow |5\rangle$ of the electronic medium can be reduced, as is already shown in figure 3, which makes the efficiency easily enhanced.

In the following, we show the conversion efficiency ρ versus the ratio g of the transition dipole moments for different energy splitting in figure 5(a). The result verifies clearly that the maximum conversion efficiency has a sensitive dependence on the ratio of the transition dipole moments. Moreover, a wide region of the maximum FWM efficiency is achieved as the ratio of the transition dipole moments is within the values ranging from 1.1 to 1.3. For further investigation into how the transition dipole moments affect the behaviour of the generated conversion efficiency, we plot the conversion efficiency ρ of the generated FWM field as a function of the two ratios of the transition dipole moments, as shown in figure 5(b). Both figures 5(a) and (b) demonstrate clearly the maximum conversion efficiency ρ is achieved at around the ratio of the transition dipole moments $g = f$. The enhancement of the generated FWM signal comes from the cross coupling caused by optical transitions between the ground and two closely separated excited states. This cross coupling modifies the neighbouring transitions and affects the multiphoton quantum destructive interference between the two different coupling pathways, thus leading to a reduction in the absorption of the pulsed probe and the generated FWM fields. We can conclude that the presence of the cross coupling modifies the linear and nonlinear optical responses of the probe pulsing transition, as well as the generated FWM process. Finally, a highly efficient FWM scheme can be achieved.

In order to further show the effects of the energy splitting Δ and the ratio g of the transition dipole moments on the conversion efficiency of the FWM field, we plot in figure 6 the conversion efficiency ρ of the generated FWM field as a function of the amplitude $|\Omega_{c2}|$ and the energy splitting Δ. Again, the results in figure 6(a) clearly show the maximum FWM efficiency is greater than 60%, when the FWM process is absolutely opened by an increase in the cw control field $|\Omega_{c2}|$. Furthermore, when the ratio of the transition dipole moment

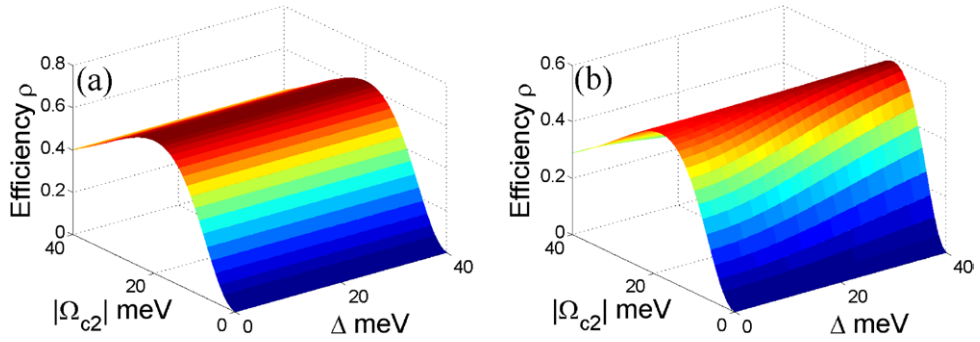

Figure 6. The conversion efficiency ρ of the generated FWM field as a function of the amplitude $|\Omega_{c2}|$ and the energy splitting Δ under the condition of (a) $g = 1.2$; (b) $g = 1.6$. The other parameter values are $\Delta = 3.5$ meV, $f = 1.2$, $L = 10$ μm, $\gamma_2 = 2 \times 10^{-5}$ meV, $\gamma_3 = \gamma_4 = 9$ meV, $\gamma_5 = 4$ meV, $\Delta_p = \Delta_{c1} = \Delta_{c2} = 0$, $\kappa_p = \kappa_p = 3\,\mu\text{m}^{-1}$ meV and $|\Omega_{c1}| = 20$ meV.

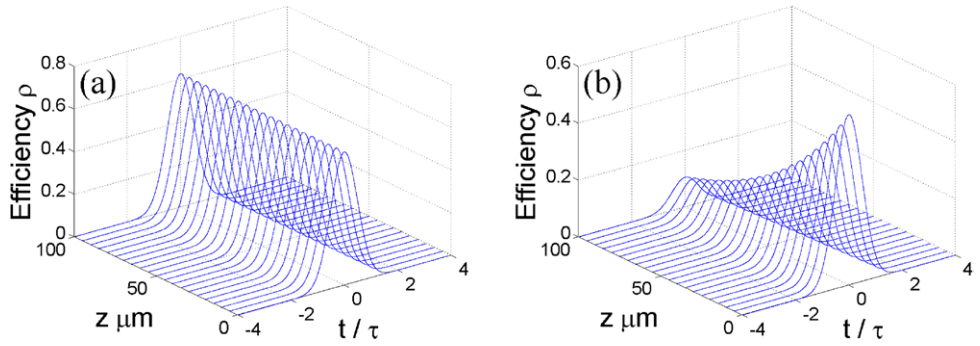

Figure 7. Surface plot of the conversion efficiency ρ as a function of time t/τ and the propagation distance z under the condition of (a) $g = 1.2$; (b) $g = 1.6$. The other parameter values are $\Delta = 3.5$ meV, $f = 1.2$, $L = 10$ μm, $\gamma_2 = 2 \times 10^{-5}$ meV, $\gamma_3 = \gamma_4 = 9$ meV, $\gamma_5 = 4$ meV, $\Delta = 3.5$ meV, $\Delta_p = \Delta_{c1} = \Delta_{c2} = 0$, $\kappa_p = \kappa_p = 3\,\mu\text{m}^{-1}$ meV and $|\Omega_{c1}| = |\Omega_{c2}| = 20$ meV.

goes from $g = 1.2$ to $g = 1.6$, as shown in figure 6(b), a similar linear increase in the conversion efficiency can be observed with an increase in the energy splitting to a certain propagation distance. Under the condition of two-photon resonance, the energy splitting between subbands $|3\rangle$ and $|4\rangle$ is employed to control the linear absorption–dispersion properties of the SQW structure, thus affecting the destructive interference between the two different coupling pathways induced by the cw control field $|\Omega_{c2}|$.

According to our analysis, the highly efficient FWM scheme may be achieved in the present SQW system via properly adjusting the system parameters. In particular, we consider the probe pulse at the entrance of the SQW structure has the form of a Gaussian pulse shape $\Omega_p(0, t) = \Omega_p(0, 0)\text{e}^{-(t/\tau)^2}$, where τ is the pulse width. The conversion efficiency can be rewritten as $\rho = \left|\Omega_m(z, t)/\Omega_p(0, 0)\right|^2$. Therefore, we present the numerical results for the analysis of the corresponding conversion FWM efficiency in figure 7. It can be clearly seen that the conversion efficiency ρ dramatically keeps its previous value as the propagation distance increases in figure 7(a). Based on the two-photon resonance, our system can cancel linear absorption and reduce the group velocity of the pulse probe and the generated FWM field. As a result, such low absorption and reduced group velocity ensure, respectively, a high FWM conversion efficiency and a long interaction time, thus leading to the enhanced FWM signal can be maintained for a long propagation distance (i.e. 100 μm). In addition, the conversion efficiency ρ decreases significantly as the ratio of the transition dipole moment $g = 1.6$, as shown in figure 7(b). The reason for the above results can be qualitatively explained as follows, the intersubband transitions $|1\rangle \leftrightarrow |3\rangle$ and $|1\rangle \leftrightarrow |4\rangle$ are suppressed due to the change in the ratio of the transition dipole moments leading to an increase in the linear absorption of the SQW medium, which is also verified in figures 2 and 3. Furthermore, this might be useful to control the transition dipole moments, thus the high conversion efficiency of the generated FWM field can remain in a long propagation distance.

4. Conclusion

In conclusion, we have suggested a giant efficient four-wave mixing scheme via two-photon resonance in asymmetric semiconductor quantum wells. Different from quantum destructive interference directly driven by the cw control field, our scheme is based on cross coupling between optical transitions induced by one weak probe pulse interacting with two cw pump fields analysed for the enhanced FWM generation. On applying the Schrödinger–Maxwell formalism, we obtain the corresponding analytical expressions of the input probe pulse and the generated FWM pulsed field in a linear regime under the steady-state condition. Considering the cross coupling in the five-subband SQW system, the main advantage of our proposed scheme is that the conversion efficiency

of FWM field is revealed to be enhanced significantly, up to 60%. Furthermore, it is worth pointing out that a wide region of the maximum FWM efficiency is demonstrated as the ratio of the transition dipole moments is within the values ranging from 1.1 to 1.3, and the generated FWM signal can be maintained for a long propagation distance due to the two-photon resonance condition. Finally, employing the advantages of flexibility and practicability in the SQW system, our scheme provides a new possibility for technological applications in such an optical modulated solid-state device.

Acknowledgments

This research is supported in part by the National Natural Science Foundation of China under Grant Nos. 11374050 and 61372102, and by the Q Lan project of Jiangsu.

References

[1] Harris S E and Hau L V 1999 *Phys. Rev. Lett.* **82** 4611
[2] Wu Y and Yang X 2005 *Phys. Rev.* A **71** 053806
[3] Petrosyan D and Malakyan Y P 2004 *Phys. Rev.* A **70** 023822
[4] Rebic S, Vitali D, Ottaviani C, Tombesi P, Artoni M, Cataliotti F and Corbalan R 2004 *Phys. Rev.* A **70** 032317
[5] Fleischhauer M, Imamoglu A and Marangos J P 2005 *Rev. Mod. Phys.* **77** 633
[6] Agarwal G S 1991 *Phys. Rev. Lett.* **67** 980
[7] Harris S E 1989 *Phys. Rev. Lett.* **62** 1033
[8] Sun H, Niu Y, Li R, Jin S and Gong S 2007 *Opt. Lett.* **32** 2475
[9] Wu J H, Gao J Y, Xu J H, Silvestri L, Artoni M, LaRocca G C and Bassani F 2005 *Phys. Rev. Lett.* **95** 057401
[10] Li J 2007 *Phys. Rev.* B **75** 155329
[11] Wang L J, Kuzmich A and Dogariu A 2000 *Nature* **406** 227
[12] Wu Y, Wen L and Zhu Y 2003 *Opt. Lett.* **28** 631
[13] Yang W X, Hou J M and Lee R K 2008 *Phys. Rev.* A **77** 033838
[14] Yang W X, Hou J M, Lin Y Y and Lee R K 2009 *Phys. Rev.* A **79** 033825
[15] Joshi A and Xiao M 2003 *Phys. Rev. Lett.* **91** 143904
[16] Yang W X, Hou J M and Lee R K 2009 *J. Mod. Opt.* **56** 716
[17] Hao X, Li J and Yang X 2009 *Opt. Commun.* **282** 3339
[18] Wu Y and Yang X 2005 *Opt. Lett.* **30** 311
[19] Wu Y and Deng L 2004 *Phys. Rev. Lett.* **93** 143904
[20] Deng L, Kozuma M, Hagley E W and Payne M G 2002 *Phys. Rev. Lett.* **88** 143902
[21] Deng L and Payne M G 2003 *Phys. Rev.* A **68** 051801
[22] Wu Y 2005 *Phys. Rev.* A **71** 053820
[23] Niu Y, Li R and Gong S 2005 *Phys. Rev.* A **71** 043819
[24] Hao X, Li J, Liu J, Song P and Yang X 2008 *Phys. Lett.* A **372** 2509
[25] Sun H, Fan S, Zhang H and Gong S 2013 *Phys. Rev.* B **87** 235310
[26] Wu Y, Payne M G, Hagley E W and Deng L 2004 *Phys. Rev.* A **69** 063803
[27] Wu Y and Yang X 2004 *Phys. Rev.* A **70** 053818
[28] Deng L and Payne M G 2003 *Phys. Rev. Lett.* **91** 243902
[29] Wu Y and Deng L 2004 *Opt. Lett.* **29** 1144
[30] Yelin S F, Sautenkov V A, Kash M M, Welch G R and Lukin M D 2003 *Phys. Rev.* A **68** 063801
[31] Zibrov A S, Ye C Y, Rostovsev Y V, Matsko A B and Scully M O 2002 *Phys. Rev.* A **65** 043817
[32] Matsko A B, Novikova I, Welch G R and Zubairy M S 2003 *Opt. Lett.* **28** 96
[33] Yan M, Rickey E and Zhu Y 2001 *Phys. Rev.* A **64** 043807
[34] Kang H, Hernandez G and Zhu Y 2004 *Phys. Rev. Lett.* **93** 073601
[35] Wu Y, Payne M G, Hagley E W and Deng L 2004 *Opt. Lett.* **29** 2294
[36] Kong L B, Wang J, Tu X H, Wen L H and Zhan M S 2005 *Opt. Commun.* **255** 331
[37] Menon S and Agarwal G S 1999 *Phys. Rev.* A **59** 740
[38] Hu Z F, Deng J L, Du C G and Wang Y Z 2008 *Commun. Theor. Phys.* **50** 961
[39] Liu H C and Capasso F 2000 *Intersubband Transitions in Quantum Wells: Physics and Device Applications* (New York: Academic)